

MOX–Report No. 44/2011

**Numerical modelling of multiphase subsurface flow in  
the presence of fractures**

FUMAGALLI,A.; SCOTTI,A.

MOX, Dipartimento di Matematica “F. Brioschi”  
Politecnico di Milano, Via Bonardi 9 - 20133 Milano (Italy)

[mox@mate.polimi.it](mailto:mox@mate.polimi.it)

<http://mox.polimi.it>



# Numerical modelling of multiphase subsurface flow in the presence of fractures

Alessio Fumagalli<sup>#</sup>, Anna Scotti<sup>#</sup>

December 15, 2011

<sup>#</sup> MOX – Modellistica e Calcolo Scientifico  
Dipartimento di Matematica “F. Brioschi”  
Politecnico di Milano  
via Bonardi 9, 20133 Milano, Italy  
alessio.fumagalli@mail.polimi.it  
anna.scotti@mail.polimi.it

**Keywords:** Multiphase Darcy flow, fractured porous media, XFEM.

**AMS Subject Classification:** 05A16, 65N38, 78M50

## Abstract

Subsurface flow is influenced by the heterogeneity of the porous medium and in particular by the presence of faults and large fractures which act as preferential paths for the flow. In this work we present a robust numerical method for the simulation of two-phase Darcy flows in heterogeneous media and propose a possible treatment of fractures by means of the extended finite element method, XFEM, and the coupling with a reduced model for the flow inside the fracture. The use of extended finite elements allows to handle fractures that are non conforming with the underlying mesh, thus increasing the applicability of the proposed scheme to the simulation of realistic problems such as oil migration in fractured basins, CO<sub>2</sub> storage or pollutant dispersion in groundwater flows.

## 1 Introduction

The study of underground flow is of great interest for its application to environmental studies, CO<sub>2</sub> sequestration, and oil field exploration and assessment. These problems are characterized by the flow of water and other fluid phases in a porous medium. Despite the high complexity of the physical phenomena, under suitable assumptions subsurface flows can be modeled as multiphase Darcy flows, [1]. In this paper we will consider a two phase Darcy model that is suitable for the simulation of oil migration, where the two immiscible phases are

oil and water, and CO<sub>2</sub> sequestration where the non-wetting phase is the supercritical CO<sub>2</sub> injected in the reservoir. One of the main difficulties in realistic simulations of Darcy flow in geophysical applications is associated to the heterogeneity of the medium. The domain of interest is indeed composed by layers of different sediments that have accumulated over millions of years and which have experienced a complex history of compaction and stress induced deformations, resulting in a strong variability of the permeability. To approximate the problem we use the mixed finite elements method with Raviart-Thomas basis functions [2], since they are robust in the presence of jumps in the permeability and they can accurately describe the velocity of the two fluids ensuring local mass conservation.

The complex stress state experienced during burial history often cause fracturing in the rocks, and fractured regions can be regarded as strongly localized heterogeneities that are very relevant for the flow. Fractures may be broadly divided into two main classes: microfractures, whose scale length is of the order of 1m, and large fractures, or faults, that extend for 100 – 1000m, with widths of some meters. While the presence of microfractures may be accounted for by averaging or homogenization techniques, leading to a change in the effective permeability [3, 4], faults may influence the flow, acting as barriers or preferential pathways, in a way that cannot be easily reproduced by a simple modification of the permeability tensor. A similar behaviour is associated to the interface between two different sedimentary layer, say a coarse sand layer and an impermeable clay layer: the surface of discontinuity, called horizon, can become a preferential path for the flow of the lighter phase thanks to buoyancy.

One possibility to address this problem is the use of a reduced model in which the fractures are represented as interfaces immersed in the porous medium, with proper coupling conditions between the fracture and the medium. The reduced model was first introduced in [5], with the assumption that the fractures behave only as preferential paths (*i.e.* they have a high permeability). Later in [6] the method was extended to handle the case of fractures acting as barriers. In [7] the relevant case of interfaces that are entirely contained in the domain is addressed. Other works on this subject are [8, 9, 10] and [11] where the two phase flow reduced model is presented for the first time.

In all the works discussed above, the fracture and the computational grid of the medium have to match, *i.e.* the fracture is a conforming interface between two mesh blocks. In realistic cases with numerous and complex fractures, mesh conformity can be a rigid constraint and even affect the quality of the mesh, with a decrease in accuracy.

In [12] the authors extend the work of [6] allowing for non matching grids between the porous domain and the fracture, increasing the flexibility of the method. Another important aspect of non matching grids is the possibility to run multiple simulations with different fractures configuration, without meshing each time the domain. Some possible fields of application are the quantification of uncertainty on geophysical parameters or multiple scenario analyses.

In this work we want to assess the effectiveness and accuracy of the reduced model for realistic problems. To this end we will evaluate the error associated with the model reduction comparing the results with those provided by the fully resolved model extending the approach presented in [12] to the case of multiple fractures with properties that can change in space. A comparison of the fully resolved model and the reduced (non-matching) approach applied to a three dimensional problem with realistic permeabilities will be made to prove that reasonably accurate results can be obtained with a coarser grid if we replace thin regions such as faults with two-dimensional interfaces.

The paper is structured as follows. In section 2 the governing equations for two-phase flow are presented together with the splitting strategy and the finite element method employed for the numerical solution. In section 3 we present the reduced model for flow along fractures and discuss the numerical method, based on the XFEM, used to solve the coupled problem with non-matching grids. Section 4 is dedicated to the discussion of numerical simulations of two phase flows in the presence of impermeable layers resolved by the grid and single phase problems with the reduced model for fractures. Finally, section 5 is devoted to conclusions.

## 2 Governing equations for two phase flows

In this section we introduce the equations governing the flow of two immiscible phases in a saturated porous medium, namely the wetting phase  $w$  and the non-wetting phase  $n$ . From now on we will indicate with the subscript  $\alpha$  quantities related to one of the two phases, *i.e.*  $\alpha \in \{w, n\}$ . The standard set of equations, derived in [13], for the two-phase flow in a porous medium describes the evolution of the saturation

$$S_\alpha = S_\alpha(\mathbf{x}, t) = \frac{\text{volume of phase } \alpha \text{ in REV}}{\text{volume of void space in REV}}, \quad (1)$$

for each phase and in each *representative elementary volume (REV)* centered in  $\mathbf{x}$  [14], the phase velocity  $\mathbf{u}_\alpha = \mathbf{u}_\alpha(\mathbf{x}, t)$  and the phase pressure  $p_\alpha = p_\alpha(\mathbf{x}, t)$ . From the definition (1) follow the constraints  $0 \leq S_\alpha \leq 1$  and  $S_n + S_w = 1$ . The system of equations that describes two-phase flow reads

$$\begin{cases} \frac{\partial (\Phi \rho_\alpha S_\alpha)}{\partial t} + \nabla \cdot (\rho_\alpha \mathbf{u}_\alpha) = \rho_\alpha q_\alpha, \\ \mathbf{u}_\alpha = -\frac{k_{r\alpha}}{\mu_\alpha} \mathbf{K} (\nabla p_\alpha - \rho_\alpha \mathbf{g}), \\ S_w + S_n = 1, \\ p_n - p_w = p_c(S_w), \end{cases} \quad \text{in } \Omega \times [0, T] \quad (2)$$

where  $\Omega$  is a bounded and regular domain in  $\mathbb{R}^d$ , with  $d = 2$  or  $3$ , and  $[0, T]$  denotes the interval of time of interest. The system must be completed with

initial data for  $\mathbf{u}_\alpha$  and  $S_\alpha$  and appropriate boundary conditions, which will be discussed later. We assume the following quantities to be given functions of space and time: the porosity  $\Phi = \Phi(\mathbf{x}, t)$  with  $0 \leq \Phi \leq 1$ , the density  $\rho_\alpha = \rho_\alpha(\mathbf{x}, t)$ , the absolute permeability tensor  $\mathbf{K} = \mathbf{K}(\mathbf{x})$ , the dynamic viscosity  $\mu_\alpha = \mu_\alpha(\mathbf{x}, t)$  and the gravity acceleration  $\mathbf{g}$ . Furthermore,  $q_\alpha = q_\alpha(\mathbf{x}, t)$  indicates a possible source term. The relative permeabilities  $k_{r\alpha} = k_{r\alpha}(S_\alpha)$ , and the capillary pressure  $p_c = p_c(S_w)$  are modeled as functions of the saturation. The first equation in (2) expresses mass conservation, while the second equation is the generalized Darcy equation, which is an approximation of the law for the conservation of momentum, see [15]. The last two equations represent the constraint on the saturations and the relation among the phase pressures and the capillary pressure respectively.

In [16] the authors propose a transformation that enables to rewrite system (2) in a more standard way, *i.e.* one parabolic equation for the saturation coupled with an elliptic equation for the pressure. This formulation is usually called *global pressure formulation* or *fractional flow formulation*. To derive the new set of equations we introduce two artificial variables: the total velocity  $\mathbf{u}$ ,

$$\mathbf{u}(\mathbf{x}, t) = \mathbf{u}_w(\mathbf{x}, t) + \mathbf{u}_n(\mathbf{x}, t), \quad (3)$$

and the global pressure  $p$ ,

$$p(\mathbf{x}, t, S_w) = p_n(\mathbf{x}, t) - \pi_w(S_w), \quad (4)$$

where

$$\pi_w(S) = \int_{S_0}^S \frac{k_{rw}(\xi)/\mu_w}{k_{rw}(\xi)/\mu_w + k_{rn}(\xi)/\mu_n} \frac{dp_c}{dS_w}(\xi) d\xi + \pi_0.$$

It is also convenient to introduce the phase mobilities  $\lambda_\alpha = k_{r\alpha}/\mu_\alpha$ , the total mobility  $\lambda = \lambda_w + \lambda_n$ , the fractional flow  $f_\alpha = \lambda_\alpha/\lambda$  and the modified gravity acceleration  $\mathbf{G} = (\lambda_w\rho_w + \lambda_n\rho_n)\mathbf{g}/\lambda$ . After some manipulations, we can rewrite the system 2 in the fractional flow formulation

$$\begin{cases} \nabla \cdot \mathbf{u} = -\frac{\partial \Phi}{\partial t} - \sum_{\alpha=n,w} \left[ \rho_\alpha^{-1} \left( \Phi S_\alpha \frac{\partial \rho_\alpha}{\partial t} + \nabla \rho_\alpha \cdot \mathbf{u}_\alpha \right) - q_\alpha \right], \\ \mathbf{u} = -\lambda \mathbf{K} (\nabla p - \mathbf{G}), \\ \frac{\partial (\Phi \rho_n S_n)}{\partial t} + \nabla \cdot (\rho_n \mathbf{u}_n) = \rho_n q_n, \\ \mathbf{u}_n = f_n \mathbf{u} - \lambda_w f_n \mathbf{K} \left[ \frac{dp_c}{dS_n} \nabla S_n + (\rho_w - \rho_n) \mathbf{g} \right], \end{cases} \quad (5)$$

in  $\Omega \times [0, T)$ . The first two equations are called *pressure equations*, while the last two are called *saturation equations*. In many groundwater applications it is normal to assume that the phase density  $\rho_\alpha$  is constant, see for instance [17, 18],

as a consequence, a simplified version of the above system can be obtained. If we introduce also the assumption that the porosity  $\Phi$  is constant the system reads

$$\begin{cases} \nabla \cdot \mathbf{u} = q_w + q_n, \\ \mathbf{u} = -\lambda \mathbf{K} (\nabla p - \mathbf{G}), \\ \Phi \frac{\partial S_n}{\partial t} + \nabla \cdot \mathbf{u}_n = q_n, \\ \mathbf{u}_n = f_n \mathbf{u} - \lambda_w f_n \mathbf{K} \left[ \frac{dp_c}{dS_n} \nabla S_n + (\rho_w - \rho_n) \mathbf{g} \right]. \end{cases} \quad \text{in } \Omega \times [0, T) \quad (6)$$

The choice of the curves for capillary pressure  $p_c$  and relative permeabilities  $k_{r\alpha}$  depends on the physical properties of the two phases and the rock. In typical applications the wetting phase is water while the non-wetting phase is a liquid or a gas. We are mostly interested in a water-liquid system, so we can use the Brooks-Corey model, introduced in [19]. The expressions of the capillary pressure and the relative permeabilities thus are

$$p_c(S_w) = p_d \bar{S}_w^{-\frac{1}{\lambda}} \quad \text{and} \quad \begin{cases} k_{rw}(S_w) = \bar{S}_w^{\frac{2+3\lambda}{\lambda}}, \\ k_{rn}(S_n) = \bar{S}_n^2 \left[ 1 - (1 - \bar{S}_n)^{\frac{2+\lambda}{\lambda}} \right], \end{cases} \quad (7)$$

where  $\lambda$  is a parameter related to the pore size distribution,  $p_d$  is the entry pressure for the porous medium,  $S_{wr} = S_{wr}(\mathbf{x})$  is the residual saturation and  $\bar{S}_\alpha$  is the effective saturation defined as

$$\bar{S}_\alpha = \frac{S_\alpha - S_{\alpha r}}{1 - S_{wr} - S_{nr}}.$$

In the case of a water-gas system instead, one could instead use the Van Genuchten model, introduced in [20]. More details on capillary pressure and relative permeabilities can be found in [14, 21].

## 2.1 The IMPlicit Pressure Explicit Saturation method

In this section we present the numerical method employed to solve the system of equations (6). Since the pressure and saturation equations are coupled the solution relies on the *IMPES* splitting (*IMP*licit *P*ressure *E*xplicit *S*aturation), [13], that splits the solution of the system (6) in two subsequent steps. At each time step we first solve the pressure equation. As the permeability depends on saturation in the two-phase case, we evaluate it using the saturation computed at the previous time step, obtaining a classic elliptic equation for pressure. The second steps consists in solving the parabolic equation for saturation where the advection velocity depends on the total Darcy velocity computed in the first step of the splitting and kept "frozen" for the time interval.

Standard continuous finite elements are not a suitable choice neither for the pressure nor the saturation equation, being designed for problems with smooth

solutions, whereas in groundwater simulations the solutions may develop sharp fronts due to convection effects. Another drawback of standard finite elements in these applications is that the velocity of the two fluids, which is critical for the coupling of the equations, is poorly approximated. More precisely, the constraint on the sum of the saturations is better satisfied if the velocity field fulfills local mass conservation. Finally the typical permeability in the equations may differ of several orders of magnitude from one grid cell to the neighboring ones, resulting in a loss of accuracy if the standard finite element method is employed. For these reasons we adopted mixed finite elements, [22], for both the pressure equation and the saturation equation, with an operator splitting technique for the latter to split its advection and diffusion part.

### 2.1.1 The pressure equation

The first two equations in the system (6), form a linear elliptic problem in mixed form for the global pressure  $p$  and the total velocity  $\mathbf{u}$ .

To solve this problem in the IMPES framework we consider a subdivision of the time interval  $[0, T]$  into  $N + 1$  sub-intervals,  $[t^k, t^{k+1})$  with  $0 = t^0 < t^1 < \dots < t^{N+1} = T$ , and we indicate with the superscript  $k$  quantities at time  $t^k$ . To solve the pressure equation we treat the total mobility  $\lambda$  and the modified gravity acceleration  $\mathbf{G}$  explicitly, thus  $\mathbf{u}$  and  $p$  are computed by solving

$$\begin{cases} \mathbf{u}^{k+1} = -\lambda(S_n^k) \mathbf{K} [\nabla p^{k+1} - \mathbf{G}(S_n^k)] , & \text{in } \Omega \\ \nabla \cdot \mathbf{u}^{k+1} = q_w + q_n , \end{cases} \quad (8)$$

for  $k = 1, 2, \dots, N$ . Dividing the boundary of the domain  $\partial\Omega$  into three disjoint parts  $\Gamma_D, \Gamma_N$  and  $\Gamma_R$  such that  $\partial\Omega = \Gamma_D \cup \Gamma_N \cup \Gamma_R$ , we can impose boundary conditions of Neumann, Dirichlet and Robin type:

$$\begin{cases} p^{k+1} = \bar{p}_N & \text{on } \Gamma_N , \\ \mathbf{u}^{k+1} \cdot \mathbf{n} = \bar{u}_D & \text{on } \Gamma_D , \\ \alpha \mathbf{u}^{k+1} \cdot \mathbf{n} - p^{k+1} = \bar{u}_R & \text{on } \Gamma_R , \end{cases}$$

where  $\bar{p}_N \in H^{1/2}(\Gamma_N)$ ,  $\bar{u}_D \in H^{-1/2}(\Gamma_D)$  and  $\bar{u}_R \in L^2(\Gamma_R)$  are given functions. To write the weak formulation of (8) we introduce the functional spaces

$$Q = L^2(\Omega) ,$$

$$\mathbf{V}_m = \{ \boldsymbol{\tau} \in H_{\text{div}}(\Omega) : \boldsymbol{\tau} \cdot \mathbf{n} = m \text{ on } \Gamma_D \text{ and } \boldsymbol{\tau} \cdot \mathbf{n} \in L^2(\Gamma_R) \}$$

and  $\mathbf{V} = \mathbf{V}_{\bar{u}_N}$ , and define the following bilinear forms and functionals

$$a(\mathbf{u}, \boldsymbol{\tau}) = \int_{\Omega} \left[ \lambda(S_n^k) \mathbf{K} \right]^{-1} \mathbf{u} \cdot \boldsymbol{\tau} + \int_{\Gamma_R} \mathbf{u} \cdot \mathbf{n} \boldsymbol{\tau} \cdot \mathbf{n} ,$$

$$b(\mathbf{u}, v) = - \int_{\Omega} \nabla \cdot \mathbf{u} v , \quad F(v) = \int_{\Omega} (q_w + q_n) v ,$$

$$G(\boldsymbol{\tau}) = \int_{\Omega} \lambda(S_n^k) \mathbf{K} \mathbf{G}(S_n^k) \cdot \boldsymbol{\tau} + \int_{\Gamma_R} \bar{u}_R \boldsymbol{\tau} \cdot \mathbf{n} - \int_{\Gamma_N} \bar{p}_N \boldsymbol{\tau} \cdot \mathbf{n} .$$

The weak formulation reads: find  $(\mathbf{u}^{k+1}, p^{k+1}) \in \mathbf{V} \times Q$  such that

$$\begin{cases} a(\mathbf{u}^{k+1}, \boldsymbol{\tau}) + b(\boldsymbol{\tau}, p^{k+1}) = G(\boldsymbol{\tau}) & \forall \boldsymbol{\tau} \in \mathbf{V}_0, \\ b(\mathbf{u}^{k+1}, v) = -F(v) & \forall v \in Q. \end{cases} \quad (9)$$

Under regularity assumptions on the data the problem is well posed, see [22]. Raviart-Thomas and discontinuous polynomial finite elements, with degree  $r$ , are used for the space approximation of velocity and pressure respectively, in particular we choose

$$\begin{aligned} Q_h &= \{v_h \in Q : v_h|_K \in \mathbb{P}_r(K) \forall K \in \mathcal{T}_h\}, \\ \mathbf{V}_h &= \{\boldsymbol{\tau}_h \in \mathbf{V} : \boldsymbol{\tau}_h|_K \in \mathbb{RT}_r(K) \forall K \in \mathcal{T}_h\}, \end{aligned}$$

where  $\mathcal{T}_h$  is a regular and conforming tessellation of  $\Omega$ . The resulting discrete system is a saddle-point problem where the global matrix is symmetric but non-defined. To recover the positivity of the matrix we use the hybridization and static condensation techniques, see [22].

### 2.1.2 The saturation equation

Let us now consider the saturation equations, *i.e.* the last two equations of the system (6), which constitute a non-linear and degenerate parabolic problem written in mixed form. Non-linearities are contained in the transport and in the diffusion terms, moreover the latter can also be degenerate if  $S_n = S_{nr}$  or  $S_n = 1 - S_{wr}$ . In the IMPES framework in each time interval  $[t^k, t^{k+1})$  from the pressure equation (8) we obtain the total velocity  $\mathbf{u}^{k+1}$ . Then, the saturation equation, valid in  $\Omega \times [t^k, t^{k+1})$ , reads

$$\begin{cases} \Phi \frac{\partial S_n}{\partial t} + \nabla \cdot \mathbf{u}_n = q_n, \\ \mathbf{u}_n = f_n \mathbf{u}^{k+1} - \lambda_w f_n \mathbf{K} \left[ \frac{dp_c}{dS_n} \nabla S_n + (\rho_w - \rho_n) \mathbf{g} \right]. \end{cases} \quad (10)$$

Dividing the boundary of the domain  $\partial\Omega$  into three disjoint parts  $\Upsilon_D$ ,  $\Upsilon_N$  and  $\Upsilon_R$  such that  $\partial\Omega = \Upsilon_D \cup \Upsilon_N \cup \Upsilon_R$ , we impose the following boundary conditions

$$\begin{cases} S_n = \bar{S}_N & \text{on } \Upsilon_N, \\ \mathbf{u}_n \cdot \mathbf{n} = \bar{u}_{n,D} & \text{on } \Upsilon_D, \\ \beta \mathbf{u}_n \cdot \mathbf{n} - S_n = \bar{u}_{n,R} & \text{on } \Upsilon_R, \end{cases} \quad (11)$$

where  $\bar{S}_N \in H^{1/2}(\Upsilon_N)$ ,  $\bar{u}_{n,D} \in H^{-1/2}(\Upsilon_D)$  and  $\bar{u}_{n,R} \in L^2(\Upsilon_R)$  are given functions. In typical groundwater applications the transport term is often dominant, so if we want to solve the equation accurately we need to use a stabilization technique. There are several possibilities, for example upwinding techniques or

operator splitting. The latter is a common approach to this type of problems, [23, 24, 25]. It is based on the splitting of the advection and diffusion operators leading to a non-linear purely hyperbolic equation and a non-linear purely diffusive parabolic equation.

The first order splitting consists in solving the hyperbolic equation first, obtaining an intermediate saturation that we call  $\widetilde{S}_n$ , then the parabolic equation with initial condition  $\widetilde{S}_n$ . The hyperbolic step has to be solved first for several reasons. First of all when we solve the hyperbolic step, we have to use boundary conditions compatible with the hyperbolic problem, *i.e.* just inflow and outflow type conditions, while the parabolic step uses the full set of boundary conditions of our problem. Furthermore the typical choice is to use an explicit scheme for the hyperbolic equation and an implicit scheme for the non-linear parabolic equation. With this splitting we obtain a global scheme which is conditionally stable and converges to the stationary solution of the problem for sufficient small time step, [26].

Based on this consideration, at each time step we first solve the hyperbolic problem, which reads

$$\begin{cases} \Phi \frac{\partial \widetilde{S}_n}{\partial t} + \nabla \cdot [f_n \mathbf{u}^{k+1} - \lambda_w f_n \mathbf{K} (\rho_w - \rho_n) \mathbf{g}] = 0, \\ \widetilde{S}_k(t^n) = S_n(t^k), \end{cases} \quad (12)$$

obtaining  $\widetilde{S}_n$  at time  $t^{k+1}$ . The boundary conditions are imposed only on the inflow part of  $\Upsilon_N$ , defining the flux as

$$\mathcal{F}(S) = f_n(S) \mathbf{u}^{k+1} - \lambda_w(S) f_n(S) \mathbf{K} (\rho_w - \rho_n) \mathbf{g},$$

then  $\widetilde{S}_n = \bar{S}_N$  on  $\Upsilon_N^{\text{inflow}} = \{ \Upsilon_N \cap \mathcal{F}(\widetilde{S}_n) \cdot \mathbf{n} > 0 \}$ . Setting

$$\widetilde{Q} = \left\{ S \in Q : S = \bar{S}_N \text{ on } \Upsilon_N^{\text{inflow}} \right\},$$

the weak formulation of the problem (12) can be written as: find  $\widetilde{S}_n \in \widetilde{Q}$  such that

$$\frac{d}{dt} \left( \Phi \widetilde{S}_n, v \right)_{L^2(\Omega)} - \left( \mathcal{F}(\widetilde{S}_n), \nabla v \right)_{L^2(\Omega)} = 0 \quad \forall v \in C_0^\infty(\Omega),$$

where  $(\cdot, \cdot)_{L^2(\Omega)}$  is the scalar product in  $L^2(\Omega)$ . The study of the well posedness of the problem is complicated and not completely solved, we refer to [27] and contained references for a preliminary analysis in the relevant case of a flux function discontinuous in space.

To solve the hyperbolic part we use the Discontinuous Galerkin method with degree  $r$ , see [28], with a suitable numerical flux. In particular, due to the heterogeneity of the medium, the flux function is discontinuous between one

grid cell and the neighboring one, so we have to carefully choose the numerical flux to satisfy the entropy condition. We refer to [29, 30, 31] for more details.

The second step of the splitting consists in solving the parabolic equation, which reads

$$\begin{cases} \Phi \frac{\partial S_n}{\partial t} + \nabla \cdot \tilde{\mathbf{u}}_n = q_n, \\ \tilde{\mathbf{u}}_n = -\lambda_w f_n \mathbf{K} \frac{dp_c}{dS_n} \nabla S_n, \end{cases} \quad \text{in } \Omega \times [t^k, t^{k+1}) \quad (13)$$

with initial data  $S_n(t^k) = \tilde{S}_n(t^{k+1})$ . The boundary conditions are defined in (11). To write the weak formulation of (13) we introduce the functional spaces

$$\mathbf{W}_m = \{ \boldsymbol{\tau} \in H_{\text{div}}(\Omega) : \boldsymbol{\tau} \cdot \mathbf{n} = m \text{ on } \Upsilon_D \text{ and } \boldsymbol{\tau} \cdot \mathbf{n} \in L^2(\Upsilon_R) \},$$

and  $\mathbf{W} = \mathbf{W}_{\tilde{u}_{n,N}}$ , and a nonlinear form and two functionals

$$\begin{aligned} w(\mathbf{u}, Z, \boldsymbol{\tau}) &= \int_{\Omega} \left[ \lambda_w(Z) f_n(Z) \mathbf{K} \frac{dp_c}{dS}(Z) \right]^{-1} \mathbf{u} \cdot \boldsymbol{\tau} + \int_{\Upsilon_R} \mathbf{u} \cdot \mathbf{n} \boldsymbol{\tau} \cdot \mathbf{n}, \\ F_S(v) &= \int_{\Omega} q_n v, \quad G_S(\boldsymbol{\tau}) = \int_{\Upsilon_R} \tilde{u}_{n,R} \boldsymbol{\tau} \cdot \mathbf{n} - \int_{\Upsilon_N} \bar{S}_N \boldsymbol{\tau} \cdot \mathbf{n}. \end{aligned}$$

The weak formulation then reads: find  $(S_n, \tilde{\mathbf{u}}_n) \in Q \times \mathbf{W}$  such that

$$\begin{cases} w(\tilde{\mathbf{u}}_n, S_n, \boldsymbol{\tau}) + b(\boldsymbol{\tau}, S_n) = G_S(\boldsymbol{\tau}) & \forall \boldsymbol{\tau} \in \mathbf{W}_0, \\ b(\tilde{\mathbf{u}}_n, v) - \frac{d}{dt} (\Phi S_n, v)_{L^2(\Omega)} = -F_S(v) & \forall v \in Q. \end{cases}$$

For the numerical solution we use the same finite element method as the pressure equation, so that, in the case of the lowest order Raviart-Thomas elements, the basis functions for the saturation  $S_n$  are the same as the basis functions for the intermediate saturation  $\tilde{S}_n$ . We handle the non-linearity in the diffusion coefficient using a quasi Newton method and employ an unconditionally stable BDF scheme for the time discretization, [32].

Since the time step for the hyperbolic part may be limited by a CFL condition, we allow for sub-iteration, see for instance [24, 33], by taking in the hyperbolic problem a time step which is a sub-multiple of the one used in the parabolic problem.

### 3 A reduced model for the flow along faults and horizons

In subsurface flow faults, horizons and large fractures can represent preferential paths for the flow. For instance during migration from the source rock to the reservoir oil tends to flow, due to buoyancy, along the interfaces between

coarse layers and the overhanging impermeable layers, or along faults. Sealed fault can also act as barriers for the flow. Although faults and fractures are often represented as surfaces they are indeed three dimensional regions with finite thickness, characterized by physical properties that differ from those of the surrounding porous medium, and should be accurately resolved by the computational grid to achieve realistic simulations. However, being the typical size of a basin  $200 \text{ Km} \times 200 \text{ Km} \times 10 \text{ Km}$  the mesh is usually too coarse to capture these features, whose characteristic dimension is of the order of some meters, unless an extreme refinement is employed, leading to unreasonably high computational times.

The alternative approach we adopt to account for these localized heterogeneities is a reduced model in which the fracture is represented by an interface immersed in the three dimensional domain. The original Darcy problem is replaced by two coupled problems for the flow within the fracture and in the surrounding domain.

In [5, 6, 7] the fracture flow equations and the proper interface conditions across the fracture were identified and mixed finite element schemes for the coupled porous medium flow / fracture flow were proposed, in the context of one phase flow. In the same framework, the authors in [12] extended the reduced model to the case in which the porous medium mesh and the fracture mesh are independent and non-matching.

If we consider, for the sake of simplicity, a two-dimensional domain cut by a thin region  $\Omega_f$  representing the fracture, as in Figure 1-a, the single phase Darcy flow is described by the following system of equations and boundary conditions

$$\left\{ \begin{array}{lll} \nabla \cdot \mathbf{u}_i = f_q & \text{in } \Omega_i, & i = 1, 2, f, \\ \mathbf{u}_i + \mathbf{K}_i \nabla p_i = \mathbf{f}_v & \text{in } \Omega_i, & i = 1, 2, f, \\ p_i = \bar{p}_i & \text{on } \Gamma_{N_i}, & i = 1, 2, f, \\ \mathbf{u}_i \cdot \mathbf{n} = \bar{g}_i & \text{on } \Gamma_{D_i}, & i = 1, 2, f, \\ \mathbf{u}_i \cdot \mathbf{n} = \mathbf{u}_f \cdot \mathbf{n} & \text{on } \gamma_i, & i = 1, 2, \\ p_i = p_f & \text{on } \gamma_i, & i = 1, 2, \end{array} \right. \quad (14)$$

where  $\mathbf{u}_i$  and  $p_i$  denote the Darcy velocity and the pressure in each subdomain respectively.

To obtain a reduced Darcy problem we replace the domain  $\Omega_f$  with an interface  $\Gamma$  and obtain the domain in Figure 1-b. If we suppose that  $\mathbf{f}_v = 0$ , that the permeability tensor is isotropic in  $\Omega_{1,2}$ , *i.e.*  $\mathbf{K}_{1,2} = k\mathbf{I}$ , and define  $\eta = k^{-1}$

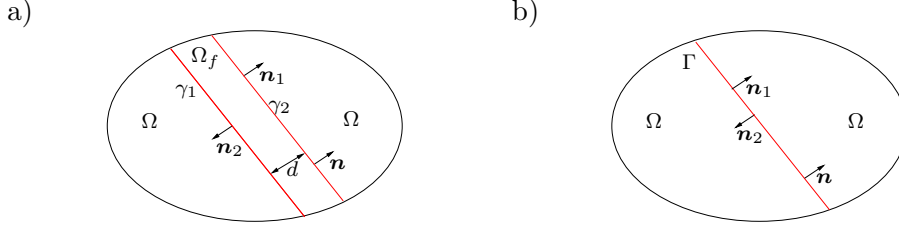


Figure 1: a) Two dimensional domain divided in two subdomains  $\Omega_{1,2}$  by a thin region  $\Omega_f$ . b) Two dimensional domain cut by an  $N - 1$  dimensional interface  $\Gamma$  that replaces the subdomain  $\Omega_f$ .

the Darcy problem in  $\Omega$  can be written as

$$\begin{cases} \nabla \cdot \mathbf{u} = f_q & \text{in } \Omega, \\ \eta \mathbf{u} + \nabla p = 0 & \text{in } \Omega, \\ p = \bar{p} & \text{on } \Gamma_N, \\ \mathbf{u} \cdot \mathbf{n} = \bar{g} & \text{on } \Gamma_D \end{cases} \quad (15)$$

with the addition of suitable conditions on  $\Gamma$ . We also assume that the permeability tensor in  $\Omega_f$  is block diagonal in local coordinates, *i.e.*  $\mathbf{K}_f = \begin{bmatrix} K_\tau & 0 \\ 0 & K_n \end{bmatrix}$  where the subscript  $\tau$  denotes the tangential directions on  $\Gamma$  and  $\mathbf{n}$  is the normal direction. If we decompose the Darcy equations in the normal and tangential components and integrate the tangential components along the thickness  $d$  of  $\Omega_f$  we obtain the reduced Darcy problem on  $\Gamma$ , namely

$$\begin{cases} \nabla_\tau \cdot \hat{\mathbf{u}} = \hat{f}_q & \text{in } \Gamma, \\ \hat{\eta} \hat{\mathbf{u}} + \nabla_\tau \hat{p} = 0 & \text{in } \Gamma, \\ \hat{p} = \bar{p} & \text{on } \Gamma \cap \Gamma_N, \\ \hat{\mathbf{u}} \cdot \mathbf{n} = \bar{g} & \text{on } \Gamma \cap \Gamma_D \end{cases} \quad (16)$$

where  $\hat{\mathbf{u}}$  is the integral of the velocity along the thickness,  $\hat{p}$  is the average pressure in the fracture and  $\hat{\eta}$  is defined as  $\hat{\eta} = (dK_\tau)^{-1}$ . The source term  $\hat{f}_q$  now accounts for the fluxes that enter the interface, being defined as  $\hat{f}_q = df_q + \llbracket \mathbf{u} \cdot \mathbf{n}_\Gamma \rrbracket$ , where we denote by  $\llbracket u \rrbracket = u_1 - u_2$  the jump of a function  $u$  that may be discontinuous across  $\Gamma$ . Finally, the interface conditions to couple the flow in  $\Omega$  and  $\Gamma$  can be obtained from the physical coupling conditions in (14) and the normal component of the equations in  $\Omega_f$  introducing assumptions on the pressure profile along the thickness of  $\Omega_f$ . The coupling conditions in the most general form, see [6], read

$$\begin{cases} \xi \mathbf{u}_1 \cdot \mathbf{n}_\Gamma + (1 - \xi) \mathbf{u}_2 \cdot \mathbf{n}_\Gamma = 2\eta_\Gamma^{-1} (p_1 - \hat{p}) & \text{on } \Gamma, \\ (1 - \xi) \mathbf{u}_1 \cdot \mathbf{n}_\Gamma + \xi \mathbf{u}_2 \cdot \mathbf{n}_\Gamma = 2\eta_\Gamma^{-1} (\hat{p} - p_2) & \text{on } \Gamma, \end{cases} \quad (17)$$

where  $\xi \in [0, 1]$  is a parameter and  $\eta_\Gamma$  is defined as  $\eta_\Gamma = dK_{\mathbf{n}}^{-1}$ . For  $\xi > \frac{1}{2}$ , these interface conditions can be rewritten as follows,

$$\begin{aligned} \eta_\Gamma \llbracket \mathbf{u} \cdot \mathbf{n}_\Gamma \rrbracket &= \frac{4}{2\xi - 1} (\{\!\{p\}\!\} - \hat{p}) && \text{on } \Gamma, \\ \eta_\Gamma \{\!\{ \mathbf{u} \cdot \mathbf{n}_\Gamma \}\!\} &= \llbracket p \rrbracket && \text{on } \Gamma, \end{aligned} \quad (18)$$

where  $\{\!\{u\}\!\} = \frac{1}{2}(u_1 + u_2)$  is the average of a function  $u$  that may be discontinuous across  $\Gamma$ .

### 3.1 The finite element approximation with non matching interfaces

The reduced model for fractures is well established in the case where the computational grid is conforming with the fractures, *i.e.* the discrete fracture consists of edges of the grid, or at most in the cases in which the nonconformity can be handled by mortaring [34]. However, the conformity of the mesh to the geometry of possibly many fracture can represent a severe constraint and affect the quality of the mesh in particular for three-dimensional realistic cases. Moreover in geophysical applications the geometry of the interfaces is often uncertain: in this framework a method that allows for nonconformities is convenient since it allows to simulate different scenarios without remeshing. We will here employ the method proposed in [12] that exploits the extended finite elements to deal with the case where some of the elements of the grid may be cut by the fracture. To this aim, we adopt the approach of enriching the finite element basis on the elements cut by the fracture with discontinuous functions. This XFEM concept, here briefly presented for reader convenience (see [12] for details), follows from the works by Hansbo *et al.* [35], [36], which however focuses on the elasticity problem in domains with fractures.

To represent solutions that are discontinuous across  $\Gamma$  we need to enrich the FEM space in the simplexes (triangles or tetrahedrons) of mesh  $\mathcal{T}_h$  that are crossed by the interface.

We consider discrete velocities  $\mathbf{v}_h$  and pressures  $q_h$  made of two components, associated to the domains  $\Omega_i$ ,  $i = 1, 2$ . The variables are defined in the following spaces,

$$\mathbf{V}_h = \mathbf{V}_{1,h} \times \mathbf{V}_{2,h} \quad \text{and} \quad Q_h = Q_{1,h} \times Q_{2,h},$$

with

$$\begin{aligned} \mathbf{V}_{i,h} &= \left\{ \mathbf{v}_h \in \mathbf{H}_{\text{div}}(\Omega_i) : \mathbf{v}_h|_{K_i} \in \mathbb{RT}_0(K_i) \forall K \in \mathcal{T}_h \right\}, \\ Q_{i,h} &= \left\{ q_h \in L^2(\Omega_i) : q_h|_{K_i} \in \mathbb{P}_0(K_i) \forall K \in \mathcal{T}_h \right\}, \end{aligned}$$

where for any  $K \in \mathcal{T}_h$   $\mathbb{RT}_0(K_i) = \left\{ \mathbf{v}_h|_{K_i} : \mathbf{v}_h \in \mathbb{RT}_0(K) \right\}$  is the linear space of the restrictions to  $K_i$  of the standard  $\mathbb{RT}_0$  local functions and  $\mathbb{P}_0(K_i)$  is

defined analogously. The discrete variables can thus be discontinuous on  $\Gamma$ , being defined on each part  $K_i$  of a cut element  $K \in \mathcal{G}_h$  by independent  $(\mathbb{RT}_0, \mathbb{P}_0)$  local functions.

### 3.2 Solving the coupled problem

The original Darcy problem in the strongly heterogeneous domain  $\Omega_1 \cup \Omega_f \cup \Omega_2$  has been replaced by two Darcy problems in  $\Omega$  and  $\Gamma$ , coupled by the interface conditions (18). The coupled problem can be solved either by direct solution of the full coupled system, or with an iterative procedure. The coupled system for the bulk and fracture flow reads

$$\begin{bmatrix} A & B^T & 0 & E \\ B & 0 & 0 & 0 \\ 0 & 0 & \hat{A} & \hat{B}^T \\ E^T & 0 & \hat{B} & 0 \end{bmatrix} \begin{bmatrix} \mathbf{u} \\ \mathbf{p} \\ \hat{\mathbf{u}} \\ \hat{\mathbf{p}} \end{bmatrix} = \begin{bmatrix} \mathbf{f}_v \\ -f_q \\ \hat{\mathbf{f}}_v \\ -\hat{f}_q \end{bmatrix}$$

where the blocks  $E$  and  $E^T$  account for the interface conditions. Since the two problems are defined on different and independent meshes in general an interpolation has to be performed between the bulk mesh  $\mathcal{T}_h$  covering  $\Omega$  and the fracture mesh  $\hat{\mathcal{T}}_h$  on  $\Gamma$ . The numerical results presented in this work were obtained by direct solution of the full system, however we point out that the iterative strategies discussed in [12], [6] are possible choices and have the clear advantage of allowing the use of different solvers and possible parallel implementation.

## 4 Numerical results

In this section we present three test cases with the aim of validating the reduced model on realistic cases and comparing it with the traditional approach. We first present in Section 4.1 a three-dimensional simulation of a two-phase flow along an impermeable fault fully resolved by the grid as our target application. In Section 4.2 we consider a synthetic two-dimensional cases and evaluate the difference between the resolved and the reduced model and finally in Section 4.3 we reformulate the problem in the first example replacing the fault with a two-dimensional interface.

### 4.1 Two-phase flow along a fracture

We present a two-phase flow for a water-liquid system, with the non-wetting phase lighter than the water, in the presence of a fracture. The fracture, which acts as a barrier, is resolved by the computational grid. Figure 2 represents a section of the domain: the computational domain is obtained by its extrusion along the  $y$  axis and has dimension  $4000 \text{ m} \times 200 \text{ m} \times 2000 \text{ m}$ . The mesh, composed by 72892 tetrahedra, is conforming with the fault and more refined therein. At initial time the medium is completely filled with water. We impose, for

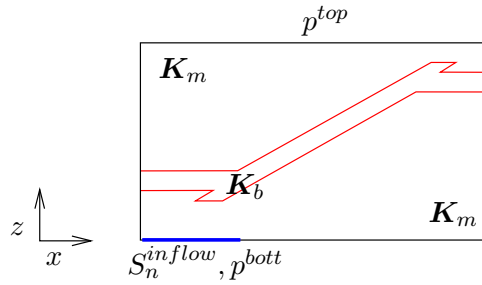


Figure 2: Schematic representation of the computational domain.

$t < 1900$  years,  $S_n^{inflow} = 0.9$  in the left part (marked in blue in Figure 2) of the bottom boundary, while it is zero on the top. We impose pressure as a natural boundary condition at the top ( $p^{top}$ ) and the bottom left part ( $p^{bott}$ ) of the domain, and homogeneous boundary conditions for the flux, for both pressure and saturation equation, on the remaining part of the boundary. The data are listed in the Table 1. Figure 3 represent the saturation  $S_n$  at two different times.

Table 1: Data for the problem of two-phase flow along a fracture.

$\mathbf{K}_m = 10^{-13} m^2$	$\mathbf{K}_b = 10^{-18} m^2$	$\mu_w = 10^{-3} Pa \cdot s$
$\mu_n = 2 \cdot 10^{-3} Pa \cdot s$	$\rho_w = 980 Kg/m^3$	$\rho_n = 700 Kg/m^3$
$S_{\alpha r} = 0$	$\lambda = 2$	$p_d = 1200 Pa$
$\Phi = 0.4$	$p^{top} = 40 MPa$	$p^{bott} = 10 MPa$

On the left, at  $t = 630$  years the saturation is higher along the fracture and fills the left and bottom part of the domain, under the impermeable layer. On the right, at  $t = 2540$  years, the inflow of saturation has stopped and light fluid has accumulated under the two impermeable layers. It can be observed also that the first accumulation starts slowly to flow along the barrier.

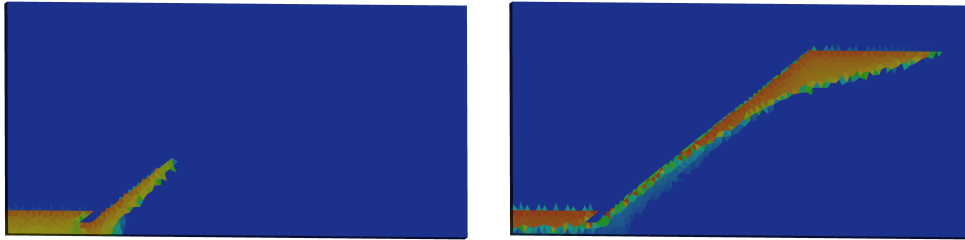


Figure 3: The saturation of the liquid at two different times: on the left at  $t = 630$  years, on the right at  $t = 2540$  years. The color scale ranges from blue,  $S_n = 0$ , to red,  $S_n = 1$ .

## 4.2 Darcy flow with two fractures - 2D case

Let us now consider some numerical examples where the presence of interfaces is accounted for with and without the reduced model.

We here consider a two-dimensional problem in a square domain cut by two fractures characterized by different properties. Let  $\Omega = [0, 1]^2$ ,  $\Gamma_1 = \{(x, y) \in \Omega : y = 0.27\}$ ,  $\Gamma_2 = \{(x, y) \in \Omega : y = 0.5x + 0.34\}$ ,  $\Gamma_D = \{0, 1\} \times [0, 1]$ , and  $\Gamma_N = [0, 1] \times \{0, 1\}$ . The bulk flow and the flow in the fracture are described by equations (15) and (16), with  $\bar{p} = y$ , and  $d = 0.05$ . We consider no flux as boundary conditions for the fractures. The source term  $f_q$  is

$$f_q = \begin{cases} 10 & \text{if } (x - 0.75)^2 + (y - 0.5)^2 < 0.04, \\ 0 & \text{otherwise.} \end{cases}$$

The first fracture, represented by  $\Gamma_1$ , is characterized by the same tangential permeability as the porous medium in  $\Omega$ , thus, if  $k = 1$  then  $\hat{\eta}_1 = d^{-1}$ , while the normal permeability is variable along the fracture,

$$\eta_{\Gamma_1} = \begin{cases} 10d & \text{if } x < 0.5, \\ 100d & \text{if } x \geq 0.5. \end{cases}$$

The second fracture, represented by  $\Gamma_2$ , is instead characterized by the same normal permeability as the porous medium in  $\Omega$ ,  $\eta_{\Gamma_2} = d$ , and a high tangential permeability, thus  $\hat{\eta}_2 = 0.01d^{-1}$ . Figure 4 shows the computational domain.

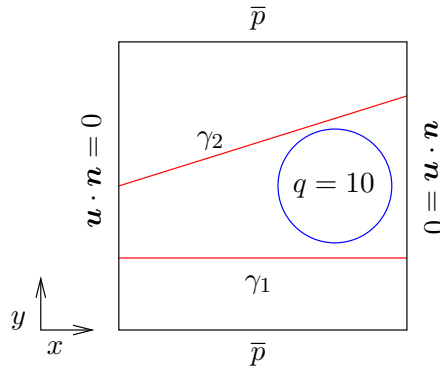


Figure 4: Computational domain cut by two interfaces.

Figure 5 shows the pressure field in  $\Omega$ ,  $\Gamma_1$  and  $\Gamma_2$ , computed with the reduced model, compared to the pressure obtained with a grid that resolves the fractures. Due to the small normal permeability of  $\Gamma_1$  there is a jump in the pressure across this fracture, and the gap changes along the line according to  $\eta_{\Gamma_1}$ . While  $\Gamma_1$  acts as a barrier for the flow  $\Gamma_2$  is a preferential path thanks to its high tangential permeability. The results are in good agreement even if the computational grid used with the reduced approach is very coarse (about 1000 triangles instead of

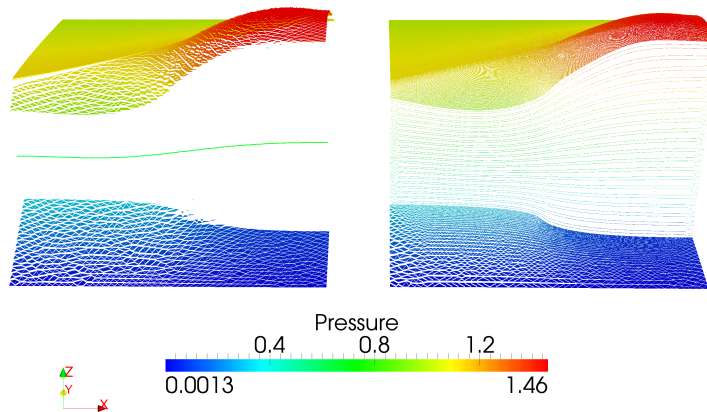


Figure 5: On the left the solution with the reduced model, with  $\xi_0 = 0.25$  and using 952 triangles and 100 elements for each fracture. On the right the reference solution with 125769 triangles.

$10^5$  for the refined case). Figure 6 shows the model error, *i.e.* the difference between the reduced model and a reference solution, taking as reference the solution of the true problem with a fine grid. Due to the model reduction the major errors are localized near the fractures, in particular when a pressure jumps occurs across a fracture. The global relative error, *i.e.* the  $L^2$  norm of

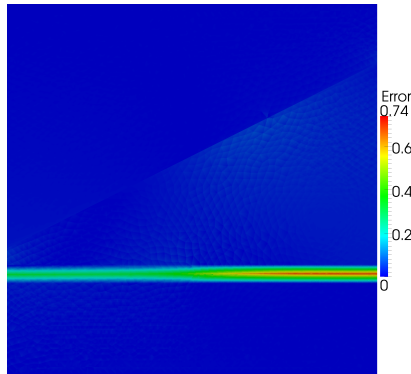


Figure 6: Model error for  $d = 0.05$  and  $\xi_0 = 0.25$ .

the model error divided by the norm of the reference solution, decreases if we reduce the width of the fractures: with  $d = 0.05$  the error is 0.0687755 while with  $d = 0.02$  the error is 0.0279828. Varying the shape parameter  $\xi_0$ , with a fixed fracture thickness  $d = 0.05$ , the relative error does not change significantly: with  $\xi_0 = 0.25$  the error is 0.0687755, with  $\xi_0 = 0$  the error is 0.0683489 while with  $\xi_0 = 0.5$  the error is 0.0691853, showing that the assumptions on the pressure profile inside the fracture has little influence on the solution outside the fracture itself.

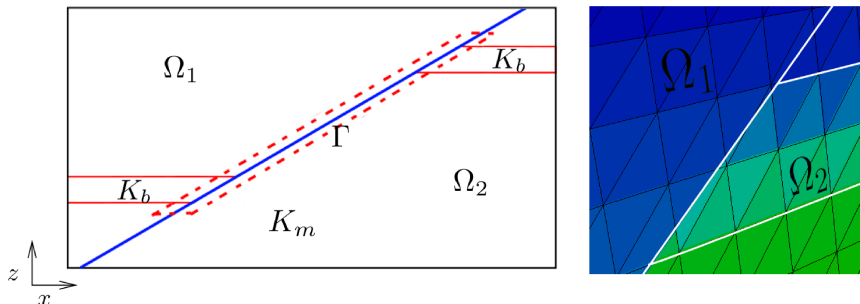


Figure 7: Schematic representation of the computational domain. The fault in Example 1 is here replaced by a two-dimensional interface. On the right a zoom of the upper impermeable layer cut by the fault: XFEM allow us to reproduce a permeability field with discontinuities within the elements of the grid.

### 4.3 Darcy flow along a fracture with the reduced model - 3D case

To assess the effectiveness of the reduced model on realistic test cases we now consider the test case in Section 4.1 and replace the fault with a two-dimensional interface. The interface  $\Gamma$  divides the domain in two subdomains  $\Omega_{1,2}$  as shown in Figure 7. We want to compare the pressure field obtained with the standard approach and a refined mesh (72892 tetrahedra) with the pressure in the matrix and in the fault computed with the reduced model with coarser grids (only 9840 tetrahedra for the matrix and 656 triangles for the fault).

The permeability field is redefined as follows

$$K(x, y, z) = \begin{cases} 10^{-15} & \text{if } 200 < z < 400 \text{ and } \mathbf{x} \in \Omega_1 \\ 10^{-15} & \text{if } 1600 < z < 1800 \text{ and } \mathbf{x} \in \Omega_2 \\ 10^{-10} & \text{otherwise} \end{cases}$$

$$K_{\Gamma,\tau}(x, y, z) = K_{\Gamma,n}(\mathbf{x}) = \begin{cases} 10^{-15} & \text{if } 750 < x < 2750 \\ 10^{-10} & \text{otherwise} \end{cases}$$

We point out that the extended finite element formulation allows us to represent a permeability coefficient  $K(x, y, z)$  that is discontinuous across  $\Gamma$  even if the grid is non conforming with the interface (Figure 7). Since the problem in Section 4.1 is a time dependent problem we here consider the pressure fields at the initial time  $t = t_0$ , *i.e.* we solve equation (8) at  $k = 0$ , with the same boundary conditions as in Table 1. Since the coupling conditions (18) refer to the case where  $\mathbf{f}_v$  is null, they should be modified to account for the effect of

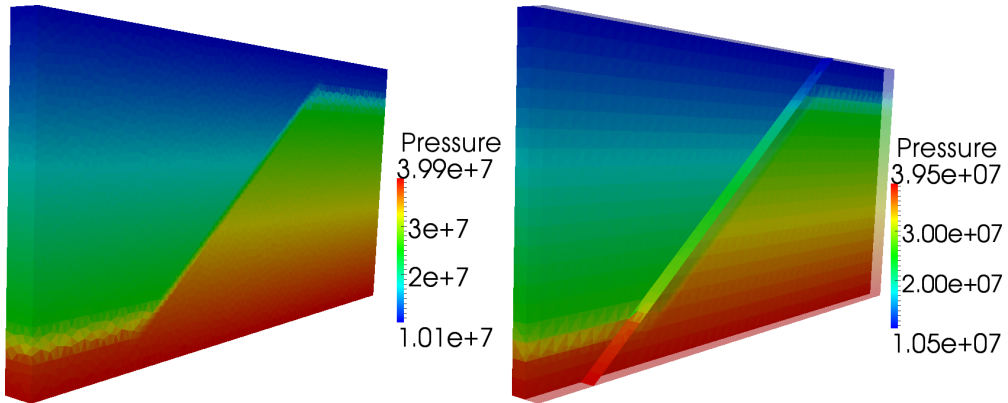


Figure 8: On the left, the pressure field of the problem in Section 4.1 at time  $t = 0$ . On the right, the pressure field computed with a coarse mesh and the reduced model for the fault. The domain is clipped at  $y = 100$  to visualize the pressure in the medium surrounding the fault.

gravity, yielding

$$\begin{aligned} \eta_{\Gamma} \llbracket \mathbf{u} \cdot \mathbf{n}_{\Gamma} \rrbracket &= \frac{4}{2\xi - 1} (\{\!\{p\}\!\} - \hat{p}) && \text{on } \Gamma, \\ \eta_{\Gamma} \{\!\{ \mathbf{u} \cdot \mathbf{n}_{\Gamma} \}\!\} + \{\!\{ \mathbf{G} \cdot \mathbf{n}_{\Gamma} \}\!\} &= \llbracket p \rrbracket && \text{on } \Gamma. \end{aligned}$$

Results are shown in Figure 8. The pressure field obtained with the fine mesh is well reproduced with the coarse mesh and the reduced model for the flow along the fault. There is a slight mismatch at the top and bottom boundary, where the imposition of the natural boundary condition is less precise with a coarse grid since pressure is approximated as piecewise constant on each tetrahedron.

The reduced model has been, so far, applied only in the single-phase case, therefore a complete comparison of the resolved and reduced approaches is not possible, nevertheless the pressure fields computed at given saturation in an IMPES framework are in good agreement. These results suggest that the presented XFEM approach could be a valuable choice for realistic problems especially if suitably extended to the multiphase case.

## 5 Conclusions and future works

The reduced model for flow along fractures and faults presented in this paper is an effective strategy to handle complex heterogeneous media with affordable computational cost. Nevertheless the method needs further improvement to be suitable for realistic simulations of multiphase flows. First of all the solution strategy developed for the saturation equation has to be extended to the case of a fractured porous medium. Since the solution of the saturation equation is based on a splitting of the hyperbolic and diffusive parts a reduced model has to

be developed for the hyperbolic part of the saturation equation in the fracture, together with a solver for the coupled hyperbolic problem in the matrix allowing for non matching grids, *i.e.* cut cells. Moreover the fault and the porous matrix are characterized by different absolute and relative permeabilities, resulting in a flux function that is discontinuous in space: numerical schemes that yield the correct entropy solution in this case are currently under study.

In realistic applications the domain is usually characterized by the presence of several faults, fractures or horizons that may intersect. These configurations, as well as the case of fractures completely immersed in the domain require an enrichment of the XFEM space with additional basis functions.

To solve real problems with complex geometries, in the high performance computing framework, we should develop scalable and robust preconditioners suitable for problems characterized by high contrast, [37].

In this paper we have presented the application of the reduced model to large scale fractures, like faults and horizons. The model is still applicable if we consider, looking at a smaller scale, a portion of the basin with micro-fractures that influence the permeability of the porous medium. The reduced model could be applied in this framework to obtain an equivalent permeability tensor in the presence of a network of fractures, as an alternative approach to be compared with the classical methods such as homogenization.

## Acknowledgements

Special thanks to Carlo D'Angelo, Franco Dassi, Luca Formaggia, Jérôme Jaffré, Michel Kern, Vincent Martin, Jean E. Roberts and Paolo Zunino for many useful discussions.

## 6 Bibliography

### References

- [1] M. Muskat, *Physical principles of oil production*. New York: McGraw-Hill Book Co., 1949.
- [2] P. A. Raviart and J. M. Thomas, A mixed finite element method for second order elliptic problems, *Lecture Notes in Mathematics*, vol. 606, pp. 292–315, 1977.
- [3] T. Arbogast, J. Douglas, Jr., and U. Hornung, Derivation of the double porosity model of single phase flow via homogenization theory, *SIAM J. Math. Anal.*, vol. 21, no. 4, pp. 823–836, 1990.
- [4] M. Kischinhevsky and P. J. Paes-leme, Modelling and numerical simulations of contaminant transport in naturally fractured porous media, *Transport in Porous Media*, vol. 26, pp. 25–49, 1997. 10.1023/A:1006506328004.

- [5] C. Alboin, J. Jaffré, J. E. Roberts, X. Wang, and C. Serres, *Domain decomposition for some transmission problems in flow in porous media*, vol. 552 of *Lecture Notes in Phys.*, pp. 22–34. Berlin: Springer, 2000.
- [6] V. Martin, J. Jaffré, and J. E. Roberts, Modeling fractures and barriers as interfaces for flow in porous media, *SIAM J. Sci. Comput.*, vol. 26, no. 5, pp. 1667–1691 (electronic), 2005.
- [7] P. Angot, F. Boyer, and F. Hubert, Asymptotic and numerical modelling of flows in fractured porous media, *M2AN Math. Model. Numer. Anal.*, vol. 43, no. 2, pp. 239–275, 2009.
- [8] J. Jaffré, V. Martin, and J. E. Roberts, Generalized cell-centered finite volume methods for flow in porous media with faults, in *Finite volumes for complex applications, III (Porquerolles, 2002)*, pp. 343–350, Hermes Sci. Publ., Paris, 2002.
- [9] N. Frih, J. E. Roberts, and A. Saada, Modeling fractures as interfaces: a model for Forchheimer fractures, *Comput. Geosci.*, vol. 12, no. 1, pp. 91–104, 2008.
- [10] N. Frih, V. Martin, J. E. Roberts, and A. Saâda, Modeling fractures as interfaces with nonmatching grids, *To appear*, 2011.
- [11] J. Jaffré, M. Mnejja, and J. Roberts, A discrete fracture model for two-phase flow with matrix-fracture interaction, *Procedia Computer Science*, vol. 4, pp. 967–973, 2011.
- [12] C. D’Angelo and A. Scotti, A Mixed Finite Element Method for Darcy Flow in Fractured Porous Media with Non-Matching Grids, *Mathematical Modelling and Numerical Analysis*, 2011. Accepted.
- [13] G. Chavent and J. Jaffré, *Mathematical Models and Finite Elements for Reservoir Simulation*, vol. 17. Elsevier, 1986.
- [14] J. Bear, *Dynamics of Fluids in Porous Media*. American Elsevier, 1972.
- [15] S. Whitaker, *The Method of Volume Averaging*, vol. 13 of *Theory and Applications of Transport in Porous Media*. Kluwer Academic Press, 1999.
- [16] G. Chavent, A new formulation of diphasic incompressible flows in porous media, in *Applications of Methods of Functional Analysis to Problems in Mechanics* (P. Germain and B. Nayroles, eds.), vol. 503 of *Lecture Notes in Mathematics*, pp. 258–270, Springer Berlin / Heidelberg, 1976. 10.1007/BFb0088761.
- [17] Z. Chen and R. E. Ewing, Comparison of various formulations of three-phase flow in porous media, *J. Comput. Phys.*, vol. 132, no. 2, pp. 362–373, 1997.
- [18] Z. Chen, G. Huan, and Y. Ma, *Computational methods for multiphase flows in porous media*. Computational Science & Engineering, Philadelphia, PA: Society for Industrial and Applied Mathematics (SIAM), 2006.

- [19] R. H. Brooks and A. T. Corey, *Hydraulic properties of porous media*. Fort Collins, CO: Civil Engineering Dept., Colorado State Univ., 1964.
- [20] M. T. van Genuchten, A closed-form equation for predicting the hydraulic conductivity of unsaturated soils, *Soil Sci. Soc. Am. J.*, vol. 44, no. 5, pp. 892–898, 1980.
- [21] Z. Chen, *Reservoir Simulation: Mathematical Techniques in Oil Recovery*, vol. 77. SIAM, 2007.
- [22] F. Brezzi and M. Fortin, *Mixed and Hybrid Finite Element Methods*, vol. 15 of *Computational Mathematics*. Springer Verlag, Berlin, 1991.
- [23] H. Holden, K. H. Karlsen, and K.-A. Lie, Operator splitting methods for degenerate convection-diffusion equations. I. Convergence and entropy estimates, in *Stochastic processes, physics and geometry: new interplays, II (Leipzig, 1999)*, vol. 29 of *CMS Conf. Proc.*, pp. 293–316, Providence, RI: Amer. Math. Soc., 2000.
- [24] H. Holden, K. H. Karlsen, and K.-A. Lie, Operator splitting methods for degenerate convection-diffusion equations ii: numerical examples with emphasis on reservoir simulation and sedimentation, *Computational Geosciences*, vol. 4, no. 4, pp. 287–322, 2000.
- [25] K. H. Karlsen, K.-A. Lie, J. R. Natvig, H. F. Nordhaug, and H. K. Dahle, Operator splitting methods for systems of convection-diffusion equations: nonlinear error mechanisms and correction strategies, *J. Comput. Phys.*, vol. 173, no. 2, pp. 636–663, 2001.
- [26] P.-L. Lions and B. Mercier, Splitting algorithms for the sum of two nonlinear operators, *SIAM J. Numer. Anal.*, vol. 16, no. 6, pp. 964–979, 1979.
- [27] C. Cancès, Asymptotic behavior of two-phase flows in heterogeneous porous media for capillarity depending only on space. II. Nonclassical shocks to model oil-trapping, *SIAM J. Math. Anal.*, vol. 42, no. 2, pp. 972–995, 2010.
- [28] B. Cockburn and C.-W. Shu, Runge-Kutta discontinuous Galerkin methods for convection-dominated problems, *J. Sci. Comput.*, vol. 16, no. 3, pp. 173–261, 2001.
- [29] J. Jaffré, Numerical calculation of the flux across an interface between two rock types of a porous medium for a two-phase flow, in *Hyperbolic problems: theory, numerics, applications (Stony Brook, NY, 1994)*, pp. 165–177, World Sci. Publ., River Edge, NJ, 1996.
- [30] Adimurthi, J. Jaffré, and G. D. Veerappa Gowda, Godunov-type methods for conservation laws with a flux function discontinuous in space, *SIAM J. Numer. Anal.*, vol. 42, no. 1, pp. 179–208 (electronic), 2004.
- [31] S. Mishra and J. Jaffré, On the upstream mobility scheme for two-phase flow in porous media, *Comput. Geosci.*, vol. 14, no. 1, pp. 105–124, 2010.

- [32] E. Hairer, S. P. Nørsett, and G. Wanner, *Solving ordinary differential equations. I*, vol. 8 of *Springer Series in Computational Mathematics*. Berlin: Springer-Verlag, second ed., 1993. Nonstiff problems.
- [33] M. S. Espedal and K. H. Karlsen, Numerical solution of reservoir flow models based on large time step operator splitting algorithms, in *Filtration in porous media and industrial application (Cetraro, 1998)*, vol. 1734 of *Lecture Notes in Math.*, pp. 9–77, Berlin: Springer, 2000.
- [34] T. Arbogast, L. C. Cowsar, M. F. Wheeler, and I. Yotov, Mixed finite element methods on nonmatching multiblock grids, *SIAM J. Numer. Anal.*, vol. 37, no. 4, pp. 1295–1315 (electronic), 2000.
- [35] A. Hansbo and P. Hansbo, An unfitted finite element method, based on Nitsche’s method, for elliptic interface problems, *Comput. Methods Appl. Mech. Engrg.*, vol. 191, no. 47-48, pp. 5537–5552, 2002.
- [36] R. Becker, E. Burman, and P. Hansbo, A Nitsche extended finite element method for incompressible elasticity with discontinuous modulus of elasticity, *Comput. Methods Appl. Mech. Engrg.*, vol. 198, no. 41-44, pp. 3352–3360, 2009.
- [37] J. Galvis and Y. Efendiev, Domain decomposition preconditioners for multiscale flows in high contrast media: reduced dimension coarse spaces, *Multiscale Model. Simul.*, vol. 8, no. 5, pp. 1621–1644, 2010.

# MOX Technical Reports, last issues

Dipartimento di Matematica “F. Brioschi”,  
Politecnico di Milano, Via Bonardi 9 - 20133 Milano (Italy)

- 44/2011 FUMAGALLI, A.; SCOTTI, A.  
*Numerical modelling of multiphase subsurface flow in the presence of fractures*
- 43/2011 L. FORMAGGIA, A. QUARTERONI, C. VERGARA  
*On the physical consistency of the coupling between three-dimensional compliant and one-dimensional problems in haemodynamics*
- 42/2011 ANTONIETTI, P.F.; QUARTERONI, A.  
*Numerical performance of discontinuous and stabilized continuous Galerkin methods or convection-diffusion problems*
- 41/2011 BURMAN, E.; ZUNINO, P.;  
*Numerical Approximation of Large Contrast Problems with the Unfitted Nitsche Method*
- 40/2011 D ANGELO, C.; ZUNINO, P.; PORPORA, A.; MORLACCHI, S.; MIGLI-  
AVACCA, F.  
*Model reduction strategies enable computational analysis of controlled drug release from cardiovascular stents*
- 39/2011 ANTONIETTI, P.F.; AYUSO DE DIOS, B.; BRENNER, S.C.; SUNG,  
L.-Y.  
*Schwarz methods for a preconditioned WOPSIP method for elliptic problems*
- 38/2011 PORPORA A., ZUNINO P., VERGARA C., PICCINELLI M.  
*Numerical treatment of boundary conditions to replace lateral branches in haemodynamics*
- 37/2011 IEVA, F.; PAGANONI, A.M.  
*Depth Measures For Multivariate Functional Data*
- 36/2011 MOTAMED, M.; NOBILE, F.; TEMPONE, R.  
*A stochastic collocation method for the second order wave equation with a discontinuous random speed*
- 35/2011 IAPICHINO, L.; QUARTERONI, A.; ROZZA, G.  
*A Reduced Basis Hybrid Method for the coupling of parametrized domains represented by fluidic networks*